Revision_1

A multi-methodological study of the (K,Ca)-variety of the zeolite merlinoite

G. Diego Gatta, Nicola Rotiroti, Danilo Bersani,
Fabio Bellatreccia, Giancarlo Della Ventura, Silvia Rizzato

Corresponding author: G. Diego GATTA

Dip. Scienze della Terra
Universita' degli Studi di Milano
Via Botticelli, 23
I-20133 Milano, Italy
Tel. +39 02 503 15607
Fax +39 02 503 15597
E-Mail: diego.gatta@unimi.it

Operating system: Windows XP

A multi-methodological study of the (K,Ca)-variety of the zeolite merlinoite

G. Diego Gatta[1,2*], Nicola Rotiroti[1], Danilo Bersani[3], Fabio Bellatreccia[4], Giancarlo Della Ventura[4], Silvia Rizzato[5]

[1]Dipartimento di Scienze della Terra, Università degli Studi di Milano, Via Botticelli 23, I-20133 Milano, Italy

[2]CNR - Istituto di Cristallografia, Sede di Bari, Via G. Amendola 122/o, I-70126 Bari, Italy

[3]Dipartimento di Fisica e Scienze della Terra, Università di Parma, Parco Area delle Scienze 7/A, I-43124 Parma, Italy

[4]Dipartimento di Scienze, Università degli Studi Roma Tre, Largo S. Leonardo Murialdo 1, I-00146 Roma, Italy

[5]Dipartimento di Chimica, Università degli Studi di Milano, Via Golgi 19, I-20133 Milano, Italy

*E-mail: diego.gatta@unimi.it

Abstract: A multi-methodological study of the (K,Ca)-variety of the zeolite merlinoite from Fosso Attici, Sacrofano (Italy), was done on the basis of electron microprobe analysis in wavelength dispersive mode (EPMA-WDS), single-crystal X-ray diffraction (at 100 K), Raman and infrared spectroscopy. The chemical formula of the merlinoite from Fosso Attici is the following: $(Na_{0.37}K_{5.69})_{\Sigma=6.06}(Mg_{0.01}Ca_{1.93}Ba_{0.40})_{\Sigma=2.34}(Fe^{3+}_{0.02}Al_{10.55}Si_{21.38})_{\Sigma=31.9}O_{64}\cdot 19.6H_2O$ (Z = 1), compatible with the ideal chemical formula: $K_6Ca_2[Al_{10}Si_{22}O_{64}]\cdot 20H_2O$.

The anisotropic structure refinements confirmed the symmetry and the framework model previously reported (space group *Immm*, with a = 14.066(5), b = 14.111(5), and c = 9.943(3) Å at 100 K). The refinement converged with four cationic sites and six H_2O molecule sites; the refined bond distances of the framework tetrahedra suggest a highly disordered Si/Al-distribution.

The Raman spectrum of merlinoite (collected between 100 and 4000 cm^{-1}) is dominated by a doublet of bands between at 496-422 cm^{-1}, assigned to the tetrahedral T-O-T symmetric bending modes. The T-O-T anti-symmetric stretching is also observed; the stretching and bending modes of the H_2O molecules are well visible only when using a blue laser.

The single-crystal near-IR spectrum shows a very weak band at 6823 cm^{-1}, assigned to the first overtone of the O-H stretching mode, and a band at 5209 cm^{-1}, due to the combination of H_2O stretching + bending modes. A very broad and convolute absorption, extending from 3700 to 3000 cm^{-1} occurs in the H_2O stretching region, while the ν_2 bending mode of H_2O is found at 1649 cm^{-1}. The powder mid-IR spectrum of merlinoite between 400-1300 cm^{-1} is dominated by tetrahedral T-O-T symmetric and anti-symmetric stretchings.

The possibility to use the Raman and FT-IR spectra of merlinoite and phillipsite as a quick identification tool for these two zeolites, which are often confused due to their close similarity, is discussed.

Keywords: merlinoite, zeolite, single crystal X-ray diffraction, Raman spectroscopy, IR spectroscopy.

Introduction

Merlinoite is a rare zeolite found in different geological environments; it has so far been described in massive volcanic rocks (Passaglia *et al*., 1977; Alberti *et al*., 1979; Khomyakov *et al*., 1981; Hentschel, 1986; Della Ventura *et al*., 1993; Yakubovich *et al*., 1999), in diagenetically-altered silicic tephra (in a lacustrine environment; Hay and Guldman, 1987), and in marine volcanic sediments (Mohapatra and Sahoo, 1987). Its ideal chemical formula was reported as $K_5Ca_2[Al_9Si_{23}O_{64}]\cdot 22H_2O$ by Coombs *et al.* (1997) and $K_6Ca_2Na[Al_{11}Si_{21}O_{64}]\cdot 22H_2O$ ($Z = 1$) by Passaglia and Sheppard (2001). K is always the dominant extraframework cation, Ca (usually ≤ 1.5 - 2 atoms per formula unit, a.p.f.u.) and Na (usually ≤ 0.6 a.p.f.u.) are present in subordinate amounts, along with Ba. In the samples of merlinoite from Cupaello (Italy) (type locality) and Sacrofano (Italy), the fraction of Ba is significant (even up to ~0.5 a.p.f.u.) (Passaglia *et al*., 1977; Della Ventura *et al*., 1993). Na-rich (*i.e*., with 5 a.p.f.u. of Na) and Ba-rich merlinoites (*i.e*., with 3 a.p.f.u. of Ba) were reported in samples from the Khibiny massif, Kola Peninsula (Russia), by Yakubovich *et al*. (1999) and Baturin *et al*. (1985), respectively.

The crystal structure of merlinoite was solved and refined by Galli *et al.* (1979) on the basis of single-crystal diffraction data from a sample from Cupaello (Italy) (previously studied and described by Passaglia *et al*., 1977). Electron microprobe analysis in wavelength dispersive mode (EPMA-WDS, with H_2O content derived by loss of ignition) of the sample used by Galli *et al.* (1979) gave the following unit formula: $(K_{4.21}Ca_{1.49}Na_{0.55}Ba_{0.43}Fe_{0.24})_{\Sigma=6.92}[Al_{9.31}Si_{22.69}]_{\Sigma=31.99}O_{64}\cdot 22.74H_2O$ (ideally $K_5Ca_2[Al_9Si_{23}O_{64}]\cdot 24H_2O$, with $Z = 1$). The structure of merlinoite was found to be orthorhombic, with space group *Immm* and $a = 14.116(7)$, $b = 14.229(6)$ and $c =$

9.946(6) Å (Galli *et al*., 1979). The tetrahedral framework of this zeolite has a **MER**-type topology (Baerlocher *et al*., 2007), with *I*4/*mmm* topological symmetry and the following idealised unit-cell parameters: a = 14.0 Å and c = 10.0 Å. The framework density is: 16 T/1000 Å^3. The **MER** framework type is built by double crankshaft chains of the feldspar type, consisting of 2-fold (1,2)-connected D4Rs. Three different secondary building units (*i.e*., 8-8 or 8 or 4) and two main building block units (*d8r (t-opr), pau (t-pau)*) are present in the **MER**-type framework (Baerlocher *et al*., 2007). Interconnecting 8-membered ring channels run parallel to [100], [010] and [001] (Fig. 1), and the 8-ring channels running parallel to [001] connect *t-pau* cages. Synthetic counterparts of merlinoite are the zeolite *Linde W* (Sherman, 1977; Bieniok *et al*., 1996), [Al-Co-P-O]-MER (Feng *et al*., 1997), [Ga-Al-Si-O]-MER (Kim *et al*., 2001),|Ba-Cl-|[Al-Si-O]-MER (Solov'eva *et al*., 1971),|K-|[Al-Si-O]-MER (Skofteland *et al*., 2001), and |NH_4-|[Be-P-O]-MER (Bu *et al*., 1998).

In their structure refinement of (natural) merlinoite, Galli *et al.* (1979) found a disordered Si/Al-distribution between the tetrahedral sites, along with five independent cationic sites (all with partial site occupancy) and eight independent H_2O sites (out of which only two with full site occupancy). The final agreement factor was R_1 = 9.3%. A further study on merlinoite from Fosso Attici, Sacrofano (Italy) was reported by Della Ventura *et al.* (1993). The material was characterised by EPMA-WDS, thermo-gravimetric (TG), X-ray powder diffraction and powder Fourier-Transform Infrared (FT-IR) analyses. The chemical formula of merlinoite from Fosso Attici is the following:

$(K_{5.02}Na_{0.66}Ba_{0.32}Sr_{0.02}Fe_{0.05}Ca_{1.60}Mn_{0.08}Mg_{0.03})_{\Sigma=7.78}[Al_{10.79}Si_{21.21}]_{\Sigma=32}O_{64}\cdot 20.10H_2O$.

Three further structural studies were performed for merlinoite species from the Khibiny massif (Russia), with the idealized formulae: $NaK_5Ba_3[Al_{12}Si_{20}O_{64}]\cdot 20H_2O$

(Baturin *et al*., 1985), $Na_5K_7[Al_{12}Si_{20}O_{64}]\cdot 24H_2O$ (Yakubovich *et al*., 1999) and $NaK_{11}[Al_{12}Si_{20}O_{64}]\cdot 15H_2O$ (Pakhomova *et al*., 2014). All the samples from Khibiny massif are (K,Na)-rich varieties of merlinoite (*sensu* Pakhomova *et al*., 2014). In the most recent study, Pakhomova *et al.* (2014) investigated the dehydration behaviour of a (K,Na)-merlinoite by means of single-crystal X-ray diffraction with step-wise heating to 225 °C, showing that merlinoite experiences a pronounced dehydration accompanied by an *Immm*-to-$P4_2/nmc$ phase transition at 75°C. A fully dehydrated phase occurs at 200°C. All the aforementioned structural investigations of (natural) merlinoite species (*i.e.*, from Italian and Russian localities) show a disordered extraframework population.

At least two further structure investigations of synthetic materials with **MER**-type framework deserve to be mentioned: 1) the $Ba_{12}Cl_8(O,OH)_4[Al_9Si_{23}O_{64}]$ (Solov'eva *et al*., 1971), which is tetragonal at room conditions (space group $I4/mmm$), and 2) the K-merlinoite (*i.e*., $K_{11.5}[Al_{11.5}Si_{20.5}O_{64}]\cdot 15H_2O$), reported by Skofteland *et al.* (2001). Skofteland *et al.* (2001) refined, by Rietveld method, the structure of the synthetic K-merlinoite at room temperature and its dehydrated form (*i.e*., $K_{11.5}[Al_{11.5}Si_{20.5}O_{64}]$) after a dehydration process at 250°C, to final $R^2_F = 0.10$ and 0.29, respectively. The *T*-induced modifications of the tetrahedral framework (mainly by polyhedral tilting) and of extraframework population were described.

Overall, the only single-crystal structure refinement of the (K,Ca)-variety of merlinoite available in the open literature is that of Galli *et al.* (1979). For the (K,Na)-variety more studies are available (*e.g*., Baturin *et al.*, 1985; Yakubovich *et al*., 1999; Pakhomova *et al*., 2014). In searching for crystals of merlinoite for non-ambient conditions experiments, we realised that the majority of samples labelled as "merlinoite" from the type locality (Cupaello, Italy) or from Sacrofano (Italy) in

several museums or private collections were actually phillipsite (and in particular twinned phillipsite; Gatta *et al.*, 2009). This can be ascribed to the similar X-ray powder diffraction patterns or optical and other physical properties of these two zeolites. In this manuscript, we report the experimental findings of a multi-methodological study on the (K,Ca)-variety of merlinoite from Fosso Attici, Sacrofano (Italy), on the basis of EPMA-WDS, single-crystal X-ray diffraction, Raman and FT-IR spectroscopy, aimed to provide a description of 1) potential structural modification in response to the applied low temperature, 2) of the Raman and IR active bands of this species and, in addition, 3) to provide a quick and reliable identification protocol by Raman and FT-IR spectroscopy.

The studied crystals were selected out from a large set (more than 40) of grains manually extracted from the same rock specimen originally studied by Della Ventura *et al.* (1993), and preliminarily tested by means of X-ray diffraction. The vast majority of these crystals turned-out to be twinned phillipsite, while only few grains turned out to be merlinoite. The crystal-chemical study of these is reported here.

Mineralogy

The merlinoite crystals described here were extracted from a volcanic ejectum collected in the upper pyroclastic level (Della Ventura *et al*., 1992) outcropping at Fosso Attici (Italy), a well-known mineralogical locality on the northern border of the Sacrofano caldera, in the Sabatini volcanic complex (De Rita *et al*., 1983), North of Rome. The host rock is a skarn product, consisting mainly of green clinopyroxene, with subordinate plagioclase and phlogopite, originating from the interaction of a magma with calcareous/dolomitic wall-rocks of the magma chamber. These tephra are

extremely porous and host secondary mineralizations in their voids, typically consisting of feldspathoids of the sodalite - hauyine group, cancrinites, grossular and vesuvianite (*e.g.*, Bellatreccia *et al*., 2005). Merlinoite occur in the studied skarn as well developed, yellowish, elongated (up to 2-3 mm) crystals with a prismatic pseudotetragonal shape, associated with phillipsite and a second zeolite-type mineral in the form of whitish spheroidal aggregates (few tenths of micrometers wide), which is still unidentified.

Experimental methods

A few millimetric crystals of merlinoite from the same rock sample were used for the EPMA-WDS analysis, X-ray diffraction and spectroscopic investigations.

Quantitative EPMA-WDS analyses were performed on a polished fragment of merlinoite (1.5 x 1.2 x 0.7 mm) using a Jeol JXA-8200 electron microprobe at the Dipartimento di Scienze della Terra, Università degli Studi di Milano (UniMI). The system was operated using a defocused electron beam (∅ 5 μm), an accelerating voltage of 15 kV, a beam current of 10 nA measured by a Faraday cup and counting times of 20s on the peaks and 5s on the backgrounds. Natural crystals of K-feldspar (for Si, K, Al), ilmenite (for Ti), forsterite (for Mg), fayalite (for Fe), wollastonite (for Ca), barite (for Ba), celestite (for Sr), and omphacite (for Na) were used as standards. The results were corrected for matrix effects using a conventional ZAF routine in the Jeol suite of programs. The crystal was found to be homogeneous within the analytical error. The chemical formula, obtained by averaging 10 point analyses and calculated on the basis of 64 oxygen atoms, is the following:

$(Na_{0.37}K_{5.69})_{\Sigma=6.06}(Mg_{0.01}Ca_{1.93}Ba_{0.40})_{\Sigma=2.34}(Fe^{3+}_{0.02}Al_{10.55}Si_{21.38})_{\Sigma=31.9}O_{64}\cdot 19.6H_2O$

(Z = 1; wt% H_2O by difference; E% = 5.5 %, Passaglia, 1970).

A fragment from the same crystal of merlinoite used for the EPMA-WDS analysis (0.18 x 0.14 x 0.08 mm) was selected for the diffraction experiment at the Dipartimento di Chimica UniMI. Single-crystal X-ray diffraction data were collected using a BRUKER-APEX II CCD diffractometer, equipped with an Oxford Cryosystems low-temperature apparatus. Data were collected using a monochromatic Mo*K*α radiation at 100 K, by using the ω-scan method (Table 1), with a counting time of 10 s per frame and a scan width of 0.5° per frame. Cell parameters were retrieved using the APEX2 software (Bruker, 2008) and refined using SAINT (Bruker, 2008) on the basis 5700 reflections. The diffraction pattern was successfully indexed with a metrically orthorhombic lattice, as previously reported for merlinoite (Galli *et al*., 1979) (Table 1). The reflection conditions suggested that the space group is *Immm*. Data reduction was performed using the SAINT software (Bruker, 2008), which corrects for Lorentz-polarization effects. Scaling and empirical absorption corrections were applied using the SADABS multi-scan method (Bruker, 2008); however, the absorption effect was not significant. The crystal was found being twinned, with a twinning law dictated by **a** and **b** approximately equal in length, emulating a tetragonal lattice [with **R** = (010,100,00-1); where **R** is the matrix that transforms the *hkl* indices of one component into the other]. A series of supplementary experiments showed that all the crystals of the sample were ubiquitously affected by twinning. The discrepancy factors between symmetry related diffraction intensities (Laue class *mmm*) was R_{int} = 0.0645 (Table 1).

A second crystal of merlinoite was used for the Raman investigation at the Dipartimento di Fisica e Scienze della Terra, Università di Parma (Italy). Single-crystal Raman spectra were collected using an Olympus BX40 microscope attached to a Jobin-Yvon Horiba LabRam confocal Raman spectrometer, equipped with a charge-

coupled detector (CCD). Spectra were collected exciting the sample with the 473.1 and the 632.81 nm laser lights, keeping the crystal with the same orientation. The laser beam was focused on the sample on a spot with nearly 2 μm of diameter (objective 50x) and the confocal aperture was set at 150 μm. The spectra were collected in backscattered geometry in the spectral range 100-4000 cm^{-1}, with 200 s counting time and 3 accumulations. The position of the Raman bands was measured using a Gauss-Lorentzian de-convolution procedure with the LabSpec v.5 software, with a precision of 0.5 cm^{-1}.

Powder infrared spectra of merlinoite were collected at the laboratory of IR spectroscopy at the Dipartimento di Scienze, Università Roma Tre (Italy), by using a Nicolet iS50 FT-IR spectrophotometer equipped with a KBr beamsplitter and a DLaTGS (Deuterated, L-alanine doped Triglycine Sulfate) detector. The spectra were collected in the 4000-400 cm^{-1} range, the nominal resolution was 4 cm^{-1} and 64 scans were averaged for both sample and background. The sample was prepared as a KBr disk by mixing 2 mg of merlinoite powder in 150 mg of KBr.

A very thin, un-oriented crystal fragment was studied by using a Bruker Hyperion 3000 FT-IR microscope (at LNF-INFN, Laboratori Nazionali, Istituto Nazionale di Fisica Nucleare, Frascati, Rome) equipped with a liquid nitrogen-cooled MCT detector attached to a VERTEX 70v FT-IR spectrophotometer. Spectra were collected using a KBr beamsplitter in the 7000-650 cm^{-1} range at the nominal resolution of 4 cm^{-1}; 128 scans were averaged for both background and sample; the beam size was ~ 50 μm.

Results: Structure refinement of merlinoite

The X-ray diffraction data of merlinoite were first processed with the programs E-STATISTICS, implemented in the WinGX package (Farrugia, 1999). The statistics of distributions of the normalized structure factors (*E*'s) showed, unambiguously, that the structure is centrosymmetric at 78% likelihood. A similar finding was obtained by the Sheldrick's $|E^2-1|$ criterion ($|E^2-1| = 0.88$). The anisotropic structure refinement was then performed in the space group *Immm* using the SHELX-97 software (Sheldrick 1997, 2008), starting from the site coordinates of merlinoite framework reported by Galli *et al.* (1979). The neutral X-ray scattering curve of Na, K, Ca, Ba, Al, Si, and O were used according to the *International Tables for Crystallography C* (Wilson and Prince, 1999). The secondary isotropic extinction effect was modeled according to the Larson's formalism (Larson, 1967), as implemented in the SHELXL-97 package (Sheldrick 1997, 2008) (Table 1). The first cycles of refinement were conducted with the framework sites only. The extraframework population was then located on the basis of the maxima in the difference-Fourier maps of the electron density; atomic coordinates, site occupancy fraction and displacement parameters of the channels population were then refined. The best model of the channels population was obtained with: *a)* one site modeled with the scattering curve of potassium (*i.e.*, *K(1)*; Fig. 2, Table 2), *b)* two mutually exclusive subsites, occupied by potassium and only ~1.1 Å apart (*i.e.*, *K(2A)* and *K(2B)*; Fig. 2, Table 2); *c)* one site occupied by calcium with partial site occupancy (*i.e.*, *C(1)*; Fig. 2, Table 2); *d)* six independent H_2O sites (*i.e.*, *W(1-6)*), out of which three with partial site occupancy (*W(4)*, *W(5)*, and *W(6)*; Fig. 2, Table 2). On the basis of the EPMA-WDS data, test cycles of refinements were performed with a mixed (K+Ba) scattering curve at the *K(1)*, *K(2A)* and *K(2B)* sites and with (Ca+Na) curve at

the *C(1)* site, but without any improvement in the figures of merit. In the last cycles of refinement, all the framework sites along with *K(1)*, *K(2A)*, and *W(1-3)* were refined anisotropically. With such a configuration, the convergence was rapidly achieved and the variance-covariance matrix showed no high correlation among the majority of the refined parameters; only for a few extraframework sites (in particular with partial occupancy) the correlation between *s.o.f.* and U_{ij} approached 75%. The displacement parameters of some extraframework sites (*i.e.*, *K(2B)*, *C(1)* and *W(3-4)*, Tables 2 and 3) reflected a positional disorder, as deduced by the inspection of the difference-Fourier map of the electron density. No peaks larger than -0.6/+0.9 $e^-/Å^3$ were present in the final difference-Fourier maps of the electron density (Table 1). The final agreement index (R_1) was 0.065 for 104 refined parameters and 1192 unique reflections with $Fo>4\sigma(Fo)$ (Table 1). Atomic coordinates and site occupancy factors are reported in Table 2, anisotropic displacement parameters in Table 3. Relevant bond lengths and angles are listed in Table 4.

Results: Raman spectrum of merlinoite

The Raman spectrum of merlinoite collected between 100 – 4000 cm^{-1} is given in Fig. 3. The lower wavenumber region is dominated by a relatively intense (very intense when excited with the blu laser) and broad band peaked at 3470 cm^{-1}, which can be assigned to the O-H stretching modes of the H_2O molecules. The bending mode of H_2O is found at 1637 cm^{-1} and is clearly visible only with the 473.1 nm laser (Fig. 3).

The lower wavenumber region (< 1200 cm^{-1}) shows only a few features: a relatively weak and broad band at 1087 cm^{-1}, a very intense doublet at 422-496 cm^{-1} and a peak at 125 cm^{-1}. A very weak absorption at 320 cm^{-1} is also barely visible. The

higher frequency peak at 1087 cm^{-1} can be assigned to the tetrahedral T-O-T symmetric stretching, whereas the 422 and 496 cm^{-1} bands can be assigned to the T-O-T symmetric bending (Dutta and Del Barco, 1985; Dutta and Puri, 1987; Wopenka *et al*., 1998; Mozgawa, 2001; Gatta *et al*., 2010).

Results: FTIR spectrum of merlinoite

The powder mid-IR spectrum of merlinoite (Fig. 4), shows, in the higher wavenumber range, a very broad absorption extending from 3700 to 3000 cm^{-1} and peaked at around 3589 cm^{-1}, which is the result of several overlapping components; these can be assigned to the stretching modes (ν_3 and ν_1) and the bending overtone ($2\nu_2$) of the H_2O molecules. The bending mode (ν_2) is observed at 1649 cm^{-1}. The lower frequency range shows a very intense and broad band centred at 1015 cm^{-1} (Fig. 4), with a pronounced shoulder at 1156 cm^{-1}, which can be assigned to the anti-symmetric stretching mode of the T-O-T bonds. Additional, well-resolved bands, occur between 820 and 540 cm^{-1} (Fig. 4); these can be assigned to the tetrahedral symmetric stretching and to vibrational modes of the rings of tetrahedra in the structure (Flanigen *et al*., 1971; Pechar, 1983; Della Ventura *et al*., 1993). A strong and broad band, which can be confidently assigned to the T-O-T bending, occurs at 425 cm^{-1}.

The single-crystal near-IR spectrum of merlinoite (Fig. 4) shows a very faint absorption at 6823 cm^{-1}, due to the first overtone of the H_2O stretching mode(s). The most intense feature in this region occurs at 5209 cm^{-1} as a broad and asymmetric band; it can be assigned to the combination ($\nu_3 + \nu_2$) of the H_2O molecules (*e.g*., Della Ventura *et al*., 2007, 2009). No bands are observed in the 4200-4800 cm^{-1} range, suggesting that no hydroxyl groups are present in merlinoite, in agreement with the

structure model of this zeolite. Assignment of the intense band at 3930 cm^{-1} is not straightforward and possibly involves the combination between internal (ν_3, ν_1) and external (translational and librational) modes of the H_2O molecule, which are usually located at low frequency (*e.g.*, Della Ventura *et al.*, 2009).

Discussion and conclusions

The EPMA-WDS data obtained in this study show that the sample from Fosso Attici, Sacrofano (Italy) is a (K,Ca)-variety of merlinoite (*sensu* Pakhomova *et al.*, 2014), with ideal chemical formula: $K_6Ca_2[Al_{10}Si_{22}O_{64}]\cdot 20H_2O$ (Table 1). If we compare the unit formula of the sample of this study with that of the (K,Ca)-merlinoite from Cupaello (Italy) reported by Galli *et al.* (1979) and Passaglia *et al.* (1977), we observe that our zeolite is richer in K (5.69 *vs.* 4.21 a.p.f.u.) and Ca (1.93 *vs.* 1.49 a.p.f.u.) and depleted in Na (0.37 *vs.* 0.55 a.p.f.u.), respectively, whereas the Ba content is virtually identical (0.40 *vs.* 0.43 a.p.f.u.). The chemical formula obtained in this study is in good agreement with the data of Della Ventura *et al.* (1993), with: 5.69 *vs.* 5.02 a.p.f.u. of K, 1.93 *vs.* 1.61 a.p.f.u. of Ca, 0.37 *vs.* 0.66 of Na, and 0.40 *vs.* 0.32 a.p.f.u. of Ba, respectively. Overall, the sample used in this study is the richest in K and Ca so far reported for the (K,Ca)-variety of merlinoite.

If we compare the unit formula of merlinoite obtained in this study on the basis of EPMA-WDS data (which appears to be of good quality in view of the low value of $E\% < 10\%$, Passaglia, 1970) with that deduced on the basis of the structure refinements (*i.e.*, $K_{6.09}Ca_{2.36}(Al,Si)_{32}O_{64}\cdot 20.7H_2O$ at 100 K), we found a reasonable agreement between EPMA-WDS and structure refinement (SR) about the electrons number of the extraframework cationic sites per formula unit: EPMA-WDS(173.3 *e*-) *vs.* SR(162.9 *e*-), with a difference of 6%. However, if we include even the electrons

number p.f.u. of the H_2O sites, we obtain virtually identical values: EPMA-WDS(330 *e*-) *vs.* SR(329 *e*-). This finding suggests that we cannot exclude a disordered distribution of cations and H_2O molecules among the extraframework sites assigned in our refinement.

The structure refinement of merlinoite from Sacrofano of this study shows a less complex configuration of the extraframework population than that of merlinoite from Cupaello reported by Galli *et al.* (1979). In our refinements, four cationic sites (*i.e.*, *K(1)*, *K2(A)*, *K(2B)* and *C(1)*, Fig. 2, Table 2) and six H_2O molecule sites (*i.e.*, *W(1-6)*, Fig. 2, Table 2) were located, whereas Galli *et al.* (1979) found five independent cationic sites (all with partial site occupancy) and eight independent H_2O sites (out of which only two with full site occupancy). In our structure model, *K(1)*, *K(2A)* and *K(2B)* sites are all located in one of the two independent 8-membered ring channels running along [001], whereas the *C(1)* is located in the other 8-membered ring channel parallel to [001], as shown in Fig. 2. The *K(1)* site is coordinated by four H_2O molecules and four framework oxygen sites (CN = 8, *K(1)*–O_{max} = 3.07 Å), the *K(2A*) site by one H_2O molecule and six O sites (CN = 7, *K(2A)*–O_{max} = 3.08 Å), the *K(2B)* site by two H_2O sites and eight O sites (CN = 10, *K(2B)*–O_{max} = 3.39 Å), and the *C(1)* site by four H_2O molecules and three O sites (CN = 7, *C(1)*–O_{max} = 3.12 Å) (Table 4). On the basis of the refined bond distances and CN, we cannot exclude that the two subsites *K(2A)* and *K(2B)*, only 1.1 Å apart and mutually exclusive, might be populated mainly by calcium and potassium, respectively. However, the use of the scattering curve of Ca to model the *K(2A)* did not improve the figures of merit of a test refinement. The structure refinement does not provide a unique picture about the Ba location: test cycles of refinement performed with a mixed (K+Ba) scattering curve at the *K(1)*, *K(2A)* and *K(2B)* sites did not lead to an improvement in the figures

of merit. However, the longest bond distances of the *K(2B)* site (Table 4) might reflect a preference of Ba for this site. Despite the intensity data were collected at 100 K (aimed to reduce the thermal effect on the atomic displacement which can be significant in this class of materials, *e.g.*, Gatta and Lotti, 2011), the refined displacement parameters of some extraframework sites (*i.e.*, *K(2B)*, *C(1)* and *W(3-4)*, Table 3) are significantly high and reflect a positional disorder (likely static), as deduced by the inspection of the difference-Fourier map of the electron density.

The structure refinement of the (K,Na)-variety of merlinoite from the Khibiny massif reported by Pakhomova *et al.* (2014) shows also a complex extraframework configuration, with eight sites modelled as occupied by K (out of which only two with *s.o.f.* > 50%) and seven H_2O sites (out of which three with *s.o.f.* > 80%).

As in all the previous structure refinements of (natural) merlinoite reported in the literature (*e.g.*, Galli *et al*., 1979; Baturin *et al*., 1985; Yakubovich *et al*., 1999; Pakhomova *et al*., 2014), also in this case the refined bond distances of the tetrahedral polyhedra suggest a highly disordered Si/Al-distribution, with $<T(1)–O> \approx <T(2)–O> \approx 1.64$ Å (Table 4).

The Raman spectrum of merlinoite is dominated by the doublet between 400 and 500 cm^{-1} (Fig. 3), tentatively assigned to the motion of oxygen atoms in the plane bisecting the T-O-T bond (*i.e.*, T-O-T bending; Dutta and Del Barco, 1985; Dutta and Puri, 1987; Wopenka *et al*., 1998; Mozgawa, 2001; Gatta *et al*., 2010). Mozgawa (2001) ascribed the Raman active bands between 400 and 600 cm^{-1} to the "breathing" vibration of 4-membered rings of tetrahedra in zeolites structure. If we compared the Raman spectrum of merlinoite and that of phillipsite (both containing 4-membered rings of tetrahedra; a collection of phillipsite spectra is available in the RRUFF database, Downs, 2006, along with those provided by Mozgawa, 2001, and Knight *et*

al., 1989), we observe a similar doublet between 400 and 500 cm^{-1}, but in merlinoite the two bands are at 422-496 cm^{-1} and in phillispite at 424-472 cm^{-1} (Mozgawa, 2001) or 424-479 cm^{-1} (Knight *et al*., 1989). In other words, the difference in wavenumber between the two peaks of the doublet is more pronounced in merlinoite ($\Delta\nu \sim 74$ cm^{-1}) than in phillipsite ($\Delta\nu \sim 52$ cm^{-1}). More specifically, the less intense band of the doublet is almost at the same wavenumber in merlinoite and in phillipsite (*i.e.*, 422-424 cm^{-1}), whereas the most intense one shows a pronounced shift (*i.e*., 496 in merlinoite and ~475 in phillipsite). The $\Delta\nu$ of the doublet between 400 and 500 cm^{-1} might be used for a quick identification of merlinoite, from the most common phillipsite, by Raman spectroscopy. The Raman spectrum of phillipsite reported by Mozgawa (2001) shows two additional bands which are not observed in the spectrum merlinoite: at 743 and 815 cm^{-1}. However, these two bands appear as weak in other spectra of phillipsite (K-, Na- and Ca-varieties) available in the open literature (Knight *et al*., 1989; Downs, 2006). In the Raman spectra of merlinoite collected in this study, the intensity of the O-H stretching mode of the H_2O molecules (*i.e*., ~ 3470 cm^{-1}, Fig. 3) is extremely sensitive to the source used to excite the sample, being much stronger when the 473.1 nm laser is used (Fig. 3), due to the different sensitivity of the detector as a function of the wavelength.

The powder mid-IR spectrum of merlinoite between 400-1300 cm^{-1} (Fig. 4) is very similar to the one reported by Della Ventura *et al.* (1993) and is dominated by the internal and external tetrahedral modes (*e.g.*, Henderson and Taylor, 1977; Della Ventura *et al*., 1993; Zecchina *et al*., 2002). In particular, the experimental spectrum of Fig. 4 confirms that the 650 - 550 cm^{-1} range, where vibrations due to the 4-membered rings of tetrahedra occur, may provide the possibility to discriminate between merlinoite from phillipsite; the former in fact shows two defined components

around 592 and 647 cm^{-1} (Fig. 4), whereas the latter shows a unique intense band at 590-600 cm^{-1} (*e.g.*, Flanigen *et al*., 1971; Della Ventura *et al*., 1993).

The single-crystal near-IR spectrum of merlinoite (Fig. 4) shows a unique and well-defined band at 5209 cm^{-1} due to the combination of H_2O stretching + bending modes. An additional absorption at 3930 cm^{-1} can be also assigned to a combination of modes involving H_2O molecules (Newman *et al*., 1986, and references therein). It is worth noting that absorptions at similar frequency are commonly observed in the near-IR spectra of zeolite-type minerals (Della Ventura *et al*., 2007).

Acknowledgements

The authors thank P. Vignola and A. Risplendente for the EPMA-WDS analysis. GDG and NR acknowledges the Italian Ministry of Education, MIUR-Project: "Futuro in Ricerca 2012 - ImPACT- RBFR12CLQD". Two anonymous reviewers and the Associate Editor S. Krivovichev are thanked.

References

Alberti, A., Hentschel, G., and Vezzalini, G. (1979) Amicite, a new natural zeolite. *Neues Jahrbuch für Mineralogie Monatshefte*, **1979**, 481–488.

Baerlocher, Ch., Meier, W.M., and Olson, D.H. (2007) Atlas of zeolite framework types, 6th ed., 398 p. Elsevier, Amsterdam, The Netherlands.

Baturin, S.V., Malinovskii, Y.A., Runovoa, I.B. (1985) Cristalline structure of the low-silica merlinoite from the Kola Peninsula. *Mineralogicheskiy Zhurnal*, **7**, 67–74 [in Russian].

Bellatreccia, F., Della Ventura, G., Libowitzky, E., Beran, A. (2005) The quantitative analysis of OH in vesuvianite: a polarized FTIR and SIMS study. *Physics and Chemistry of Minerals*, **32**, 65-76.

Bieniok, A., Bornholdt, K., Brendel, U., and Baur, W.H. (1996) Synthesis and crystal structure of zeolite W, resembling the mineral merlinoite. *Journal of Materials Chemistry*, **6**, 271–275.

Bruker (2008) *APEX2*, *SAINT* and *SADABS,* Bruker AXS Inc., Madison, Wisconsin, USA.

Bu, X., Gier, T.E., and Stucky, G.D. (1998) Hydrothermal synthesis and low temperature crystal structure of an ammonium beryllophosphate with the merlinoite topology. *Microporous and Mesoporous Materials*, **26**, 61–66.

Coombs, D.S, Alberti A., Armbruster T., Artioli G., Colella C., Grice J.D., Galli E., Liebau F., Minato H., Nikel E.H., Passaglia E., Peacor D.R., Quartieri S., Rinaldi R., Ross M., Sheppard R. A., Tillmans E., and Vezzalini G. (1997) Recommended Nomenclature for Zeolite Minerals: Report of the Subcommittee on Zeolite of the International Mineralogical Association Commission on New Minerals and Mineral Names. *The Canadian Mineralogist*, **35**, 1571-1606.

Della Ventura, G., Parodi, G.C., Burragato, F., and Mottana, A. (1993) Nuovi dati sulla merlinoite e su zeoliti affini. *Rendiconti Lincei*, **4**, 303–313.

Della Ventura, G., Di Lisa, A., Marcelli, M., Mottana, A., Paris, E. (1992) Composition and structural state of alkali feldspars from ejecta in the Roman potassic province, Italy; petrological implications. *European Journal of Mineralogy*, **4**, 411-424.

Della Ventura, G., Bellatreccia, F., Parodi, G.C., Cámara, F., Piccinini, M. (2007) Single-crystal FTIR and X-ray study of vishnevite, ideally $[Na_6(SO_4)][Na_2(H_2O)_2](Si_6Al_6O_{24})$. *American Mineralogist*, **92**, 713-721.

Della Ventura, G., Gatta, D., Redhammer, G., Bellatreccia, F., Loose, A., Parodi, G.C. (2009) Single-crystal polarized FTIR spectroscopy and neutron diffraction refinement of cancrinite. *Physics and Chemistry of Minerals*, **36**, 193-206.

De Rita, D., Funiciello, R., Rossi, U., Sposato, A. (1983) Structure and evolution of the Sacrofano Baccano caldera, Sabatini volcanic complex, Rome. *Journal of Volcanology and Geothermal Resources*, **17**, 219-236

Downs, R.T. (2006) The RRUFF Project: an integrated study of the chemistry, crystallography, Raman and infrared spectroscopy of minerals (http://rruff.info/). Program and Abstracts of the 19th General Meeting of the International Mineralogical Association in Kobe, Japan, O03-13.

Dutta, P.K. and Del Barco, B. (1985) Structure-sensitive Raman bands in hydrated zeolite A. *Journal of the Chemical Society - Chemical Communications*, **1985**, 1297-1299.

Dutta, P.K. and Puri, M. (1987) Synthesis and structure of zeolite ZSM-5: a Raman spectroscopic study. *Journal of Physical Chemistry*, **91**, 4329–4333.

Farrugia, L.J. (1999) WinGX suite for small-molecule single-crystal crystallography. *Journal of Applied Crystallography*, **32**, 837-838.

Feng, P., Bu, X. and Stucky, G.D (1997) Hydrothermal syntheses and structural characterization of zeolite analogue compounds based on cobalt phosphate. *Nature*, **388**, 735-741.

Flanigen, E.M., Khatami, H., Szymanski, H.A. (1971) Infrared structural studies of zeolite frameworks. In Molecular Sieve Zeolites-I, Vol. 101, p. 201-229. Advances in Chemistry, American Chemical Society.

Galli, E., Gottardi, G., and Pongiluppi, D. (1979) The crystal structure of the zeolite merlinoite. *Neues Jahrbuch für Mineralogie Monatshefte*, **1979**, 1–9.

Gatta, G.D., Cappelletti, P., Rotiroti, N., Slebodnick, C., and Rinaldi, R. (2009) New insights into the crystal structure and crystal chemistry of the zeolite phillipsite. *American Mineralogist*, **94**, 190-199.

Gatta, G.D., Kahlenberg, V., Kaindl, R., Rotiroti, N., Cappelletti, P., and de' Gennaro, M. (2010) Crystal-structure and low-temperature behavior of "disordered" thomsonite. *American Mineralogist*, **95**, 495-502.

Gatta, G.D. and Lotti, P. (2011) On the low-temperature behavior of the zeolite gobbinsite: A single-crystal X-ray diffraction study. *Microporous and Mesoporous Materials*, **143**, 467–476.

Hay, R.L. and Guldman, S.G. (1987) Diagenetic alteration of silicic ash in Searles Lake, California. *Clays & Clay Minerals*, **35**, 449-457.

Henderson, C.M.B. and Taylor, D. (1977) Infrared spectra of anhydrous members of the sodalite family. *Spectrochimica Acta A*, **33**, 283-290.

Hentschel, G. (1986) Paulingit und andere seltene Zeolithe in einem gefritteten Sandsteineinschluss im Basalt von Ortenberg (Vogelsberg, Hessen). *Geologisches Jahrbuch Hessen*, **114**, 249–256.

Khomyakov, A.P., Kurova, T.A., and Muravishkaya, G.I. (1981) Merlinoite, first occurrence in the USSR. *Transactions (Doklady) of the USSR Academy of Sciences, Earth Science Sections*, **256**, 172–174.

Kim, S.H., Kim, S.D., Kim, Y.C., Kim, C.S. and Hong, S.B. (2001) Synthesis and characterization of Ga-substituted MER-type zeolites. *Microporous and Mesoporous Materials*, **42**, 121-129.

Knight, C.L., Williamson, M.A., and Bodnar, R.J. (1989) Raman spectroscopy of zeolites: Characterization of natural zeolites with the laser Raman microprobe. In

P.E. Russell, Ed., *Microbeam Analysis – 1989*, p. 571-573. San Francisco Press, San Francisco CA-U.S.A..

Larson, A.C. (1967) Inclusion of secondary extinction in least-squares calculations. *Acta Crystallographica*, **23**, 664 – 665.

Mohapatra, B.K. and Sahoo, R.K. (1987) Merlinoite in manganese nodules from the Indian Ocean. *Mineralogical Magazine*, **51**, 749–750.

Mozgawa, W. (2001) The relation between structure and vibrational spectra of natural zeolites. *Journal of Molecular Structure*, **596**, 129-137.

Newmann, S., Stolper, E.M. and Epstein, S. (1986) Measurements of water in rhyolitic glasses: Calibration of an infrared spectroscopic technique. *American Mineralogist*, **71**, 1527-1541.

Pakhomova, A.S., Armbruster T., Krivovichev, S.V., and Yakovenchuk, V.N. (2014) Dehydration of the zeolite merlinoite from the Khibiny massif, Russia: an in situ temperature-dependent single-crystal X-ray study. *European Journal of Mineralogy*, **26**, 371–380.

Passaglia, E. (1970) The crystal chemistry of chabazites. *American Mineralogist*, **55**, 1278-1301.

Passaglia, E., Pongiluppi, D., and Rinaldi, R. (1977) Merlinoite, a new mineral of the zeolite group. *Neues Jahrbuch für Mineralogie Monatshefte*, **1977**, 355–364.

Passaglia, E. and Sheppard, R.A. (2001) The crystal chemistry of zeolites. In D.L. Bish and D.W. Ming, Eds., Natural zeolites: occurrence, properties, application, Vol. 45, p. 69-116. Reviews in Mineralogy and Geochemistry, Mineralogical Society of America and Geochemical Society, Washington, U.S.A.

Pechar, F. (1983) Infrared reflection of selected natural zeolites. *Neues Jahrbuch für Mineralogie Monatshefte*, **1983**, 335-364.

Sheldrick, G.M. (1997) *SHELX-97 – A program for crystal structure refinement*. University of Göttingen, Göttingen.

Sheldrick, G.M. (2008) A short history of *SHELX*. *Acta Crystallographica*, **A64**, 112-122.

Sherman, J.D. (1977) Identification and characterization of zeolites synthesized in the K_2O-Al_2O_3-SiO_2-H_2O system. In J.R. Katzer, Ed., Molecular Sieves II, ACS Symp. Ser. 40, American Chemical Society, Washington, 30–42.

Skofteland, B.M., Ellestad, O.H., and Lillerud, K.P. (2001) Potassium merlinoite: crystallization, structural and thermal properties. *Microporous and Mesoporous Materials*, **43**, 61–71.

Solov'eva, L.P., Borisov, S.V., and Bakakin, V.V. (1971) New skeletal structure in the crystal structure of barium chloroaluminosilicate $BaAlSi_2O_6(Cl,OH) \rightarrow Ba_2[X]BaCl_2[(Si,Al)_8O1_8$. *Kristallografiya*, **16**, 1179.

Wopenka, B., Freeman, J.J., and Nikischer, T. (1998) Raman spectroscopic identification of fibrous natural zeolites. *Applied Spectroscopy*, **52**, 54-63.

Wilson, A.J.C. and Prince, E. (1999) *International Tables for Crystallography Vol. C, Mathematical, Physical and Chemical Tables*, second ed., Kluwer, Dordrecht.

Yakubovich, O.V., Massa, W., Pekov, I.V., and Kucherinenko, Y.V. (1999) Crystal structure of a Na,K-variety of merlinoite. *Crystallographic Report*, **44**, 776–782.

Zecchina, A., Spoto, G., and Bordiga, S. (2002) Vibrational Spectroscopy of Zeolites. In John M. Chalmers and Peter R. Griffiths, Eds., Handbook of Vibrational Spectroscopy, Vol. 4, p. 3042–3071. John Wiley & Sons Ltd, Chichester (UK).

Table 1. Details pertaining to the data collection and structure refinement of merlinoite.

Crystal size (mm)	0.18 x 0.14 x 0.08
Cell parameters	a = 14.066(5) Å
	b = 14.111(5) Å
	c = 9.943(3) Å
Space group	*Immm*
Reference formula	$K_6Ca_2Al_{10}Si_{22}O_{64}{\cdot}20H_2O$
Z	1
Radiation (Å)	Mo$K\alpha$
T (K)	100
Scan type, steps and width:	
type	ω-scan
time per step (s)	10
width (°)	0.5
Max. 2θ (°)	60
	$-19 \le h \le 19$
	$-19 \le k \le 19$
	$-13 \le l \le 13$
Calculated density (g/cm^3)	2.177
Absorption coefficient (μ, mm^{-1})	1.12
Volume of the two individuals (%)	40, 60
Extinction coefficient	0.009(6)
No. measured reflections	8479
No. unique reflections	1304
No. unique refl. with $F_o > 4\sigma(F_o)$	1192
No. refined parameters	104
R_σ	0.0451
R_{int}	0.0645
R_1 (F) with $F_o > 4\sigma(F_o)$	0.0653
wR_2 (F^2), all reflections	0.1087
Weighting Scheme: a, b	0.01, 0
Residuals (e^-/Å^3)	-0.61/+0.96

Notes: The crystal was found being twinned, with a twinning law dictated by **a** and **b** approximately equal in length, emulating a tetragonal lattice [with **R** = (010,100,00-1); where **R** is the matrix that transforms the *hkl* indices of one component into the other]. The volume fraction of the two individuals was refined.

$R_\sigma = \Sigma\,[\sigma\,(F_{obs}^2)\,] / \Sigma\,[\,F_{obs}^2\,]$; $R_{int} = \Sigma\,|\,F_{obs}^2 - F_{obs}^2(\text{mean})\,| / \Sigma\,[\,F_{obs}^2\,]$;
$R_1 = \Sigma||F_{obs}| - |F_{calc}||/\Sigma|F_{obs}|$; $wR_2 = [\Sigma[w(F^2_{obs} - F^2_{calc})^2]/\Sigma[w(F^2_{obs})^2]]^{0.5}$;
$w = 1/\,[\sigma^2(F_{obs}^2) + (a*P)^2 + b*P\,]$; $P = (\text{Max}\,(F_{obs}^2, 0) + 2*F_{calc}^2)/3$.

Table 2. Refined fractional atomic coordinates, site occupancy factors (*s.o.f.*), and equivalent isotropic temperature factors (Å^2) based on the X-ray diffraction data collected at 100 K. U_{eq} is defined as one third of the trace of the orthogonalised U_{ij} tensor.

Site	*s.o.f.*	*x*	*y*	*z*	U_{eq}/U_{iso}
T(1)	Si, 1	0.10986(9)	0.24707(9)	0.15480(12)	0.0132(3)
T(2)	Si, 1	0.28436(9)	0.11015(9)	0.15868(11)	0.0129(3)
O(1)	O, 1	0.1250(4)	0.2845(3)	0	0.0211(11)
O(2)	O, 1	0.3137(4)	0.1169(4)	0	0.0236(12)
O(3)	O, 1	0	0.2101(4)	0.1794(5)	0.0250(12)
O(4)	O, 1	0.2793(4)	0	0.2108(5)	0.0239(12)
O(5)	O, 1	0.1788(3)	0.1572(3)	0.1889(3)	0.0254(8)
O(6)	O, 1	0.3682(3)	0.1639(3)	0.2441(4)	0.0275(8)
K(1)	K, 0.815(11)	0.1538(2)	0.5	0	0.0355(11)
K(2A)	K, 0.579(11)	0.5	0.1874(4)	0	0.0309(15)
K(2B)	K, 0.128(17)	0.5	0.269(3)	0	0.092(18)
C(1)	Ca, 0.295(11)	0.0858(10)	0	0.2628(17)	0.106(6)
W(1)	O, 1	0	0.5	0.1766(8)	0.0283(17)
W(2)	O, 1	0.5	0	0	0.042(3)
W(3)	O, 1	0.1705(19)	0.118(2)	0.5	0.272(13)
W(4)	O, 0.57(4)	0.083(3)	0	0	0.131(16)
W(5)	O, 0.22(2)	0.036(2)	0	0.176(3)	0.051(11)
W(6)	O, 0.33(3)	0.1042(16)	0	0.351(2)	0.052(8)

Table 3. Refined displacement parameters (Å^2) in the expression: $-2\pi^2[(ha^*)^2U_{11} + \ldots + 2hka^*b^*U_{12} + \ldots + 2klb^*c^*U_{23}]$, based on the X-ray data collected at 100 K.

	U_{11}	U_{22}	U_{33}	U_{12}	U_{13}	U_{23}
T(1)	0.0120(5)	0.0140(6)	0.0137(5)	0.0005(5)	-0.0005(5)	-0.0026(5)
T(2)	0.0174(6)	0.0098(6)	0.0116(5)	0.0012(5)	-0.0011(5)	-0.0013(5)
O(1)	0.025(3)	0.022(3)	0.016(2)	-0.005(2)	0	0
O(2)	0.031(3)	0.016(2)	0.023(2)	0.002(2)	0	0
O(3)	0.020(3)	0.027(3)	0.028(3)	0	0	0.006(2)
O(4)	0.035(3)	0.014(2)	0.023(2)	0	0.005(2)	0
O(5)	0.020(2)	0.025(2)	0.032(2)	0.009(2)	0.004(1)	0.003(2)
O(6)	0.031(2)	0.022(2)	0.029(2)	0.002(2)	-0.006(2)	-0.010(2)
K(1)	0.029(2)	0.054(2)	0.023(2)	0	0	0
K(2A)	0.022(2)	0.047(3)	0.025(2)	0	0	0
W(1)	0.019(4)	0.011(3)	0.055(5)	0	0	0
W(2)	0.012(5)	0.047(8)	0.066(8)	0	0	0
W(3)	0.24(2)	0.41(4)	0.16(2)	-0.01(3)	0	0

Table 4. Relevant bond distances (Å) and angles (°) based on the X-ray structure refinement at 100 K.

T(1) - O(1)	1.641(2)
T(1) - O(3)	1.649(2)
T(1) - O(5)	1.632(4)
T(1) - O(6)	1.638(4)
<T(1) - O>	1.640
T(2) - O(2)	1.634(2)
T(2) - O(4)	1.640(2)
T(2) - O(5)	1.654(4)
T(2) - O(6)	1.639(4)
<T(2) - O>	1.642
K(1) - W(1) x 2	2.787(6)
K(1) - W(3) x 2	2.98(3)
K(1) - O(4) x 2	3.026(5)
K(1) - O(1) x 2	3.068(5)
K(2A) - W(2)	2.645(6)
K(2A) - O(2) x 2	2.803(6)
K(2A) - O(6) x 4	3.073(4)
K(2B) - W(3) x 2	2.88(4)
K(2B) - O(3) x 2	3.201(7)
K(2B) - O(2) x 2	3.39(3)
K(2B) - O(6) x 4	3.39(2)
C(1) - O(5) x 2	2.677(8)
C(1) - W(4)	2.61(2)
C(1) - O(4)	2.77(1)
C(1) - W(6)	2.81(3)
C(1) - W(3) x 2	3.12(2)
O(1)-T(1)-O(3)	111.2(3)
O(1)-T(1)-O(5)	111.6(3)
O(1)-T(1)-O(6)	107.7(3)
O(3)-T(1)-O(5)	106.3(2)
O(3)-T(1)-O(6)	109.2(2)
O(5)-T(1)-O(6)	110.9(2)
<O-T(1)-O>	109.5
O(2)-T(2)-O(4)	111.8(3)
O(2)-T(2)-O(5)	112.3(2)
O(2)-T(2)-O(6)	107.0(3)
O(4)-T(2)-O(5)	106.5(3)
O(4)-T(2)-O(6)	107.8(3)
O(5)-T(2)-O(6)	111.5(2)
<O-T(2)-O>	109.5

Figure 1. The tetrahedral framework of merlinoite viewed down [100], [010], and [001]. Interconnecting 8-membered ring channels run parallel to [100], [010] and [001].

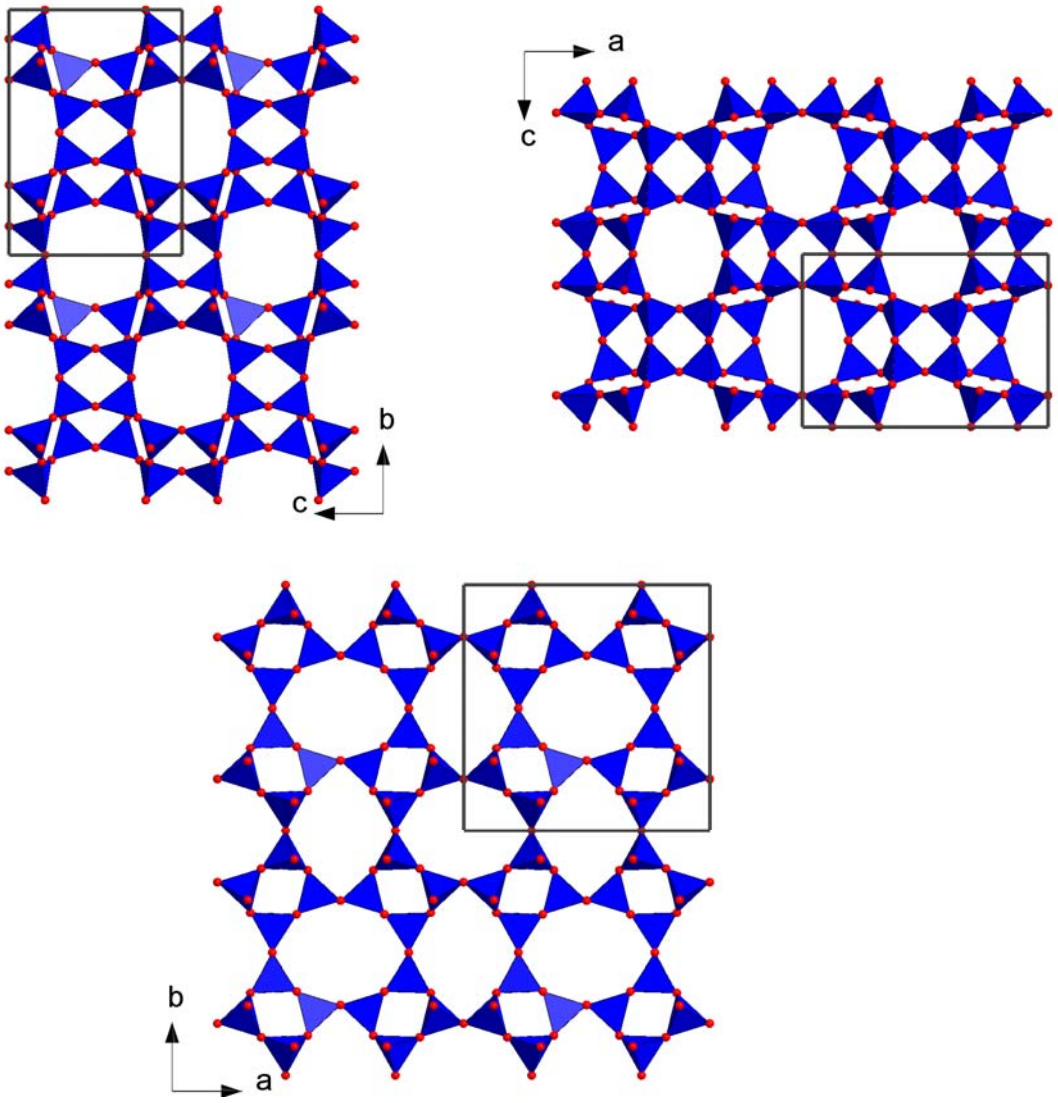

Figure 2. A view of the crystal structure of merlinoite down [001] based on the structure refinement of this study. The extraframework sites are labelled according to Table 2.

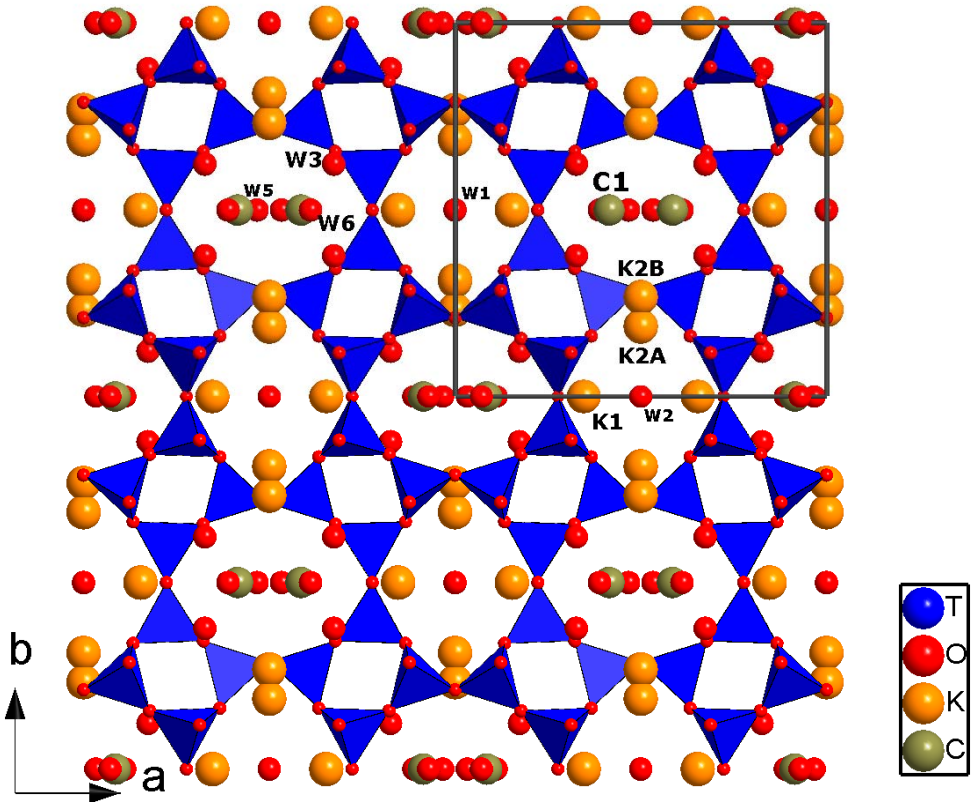

Figure 3. Single-crystal Raman spectra of merlinoite collected with the 473.1 and the 632.8 nm laser lights, respectively, keeping the crystal with the same orientation.

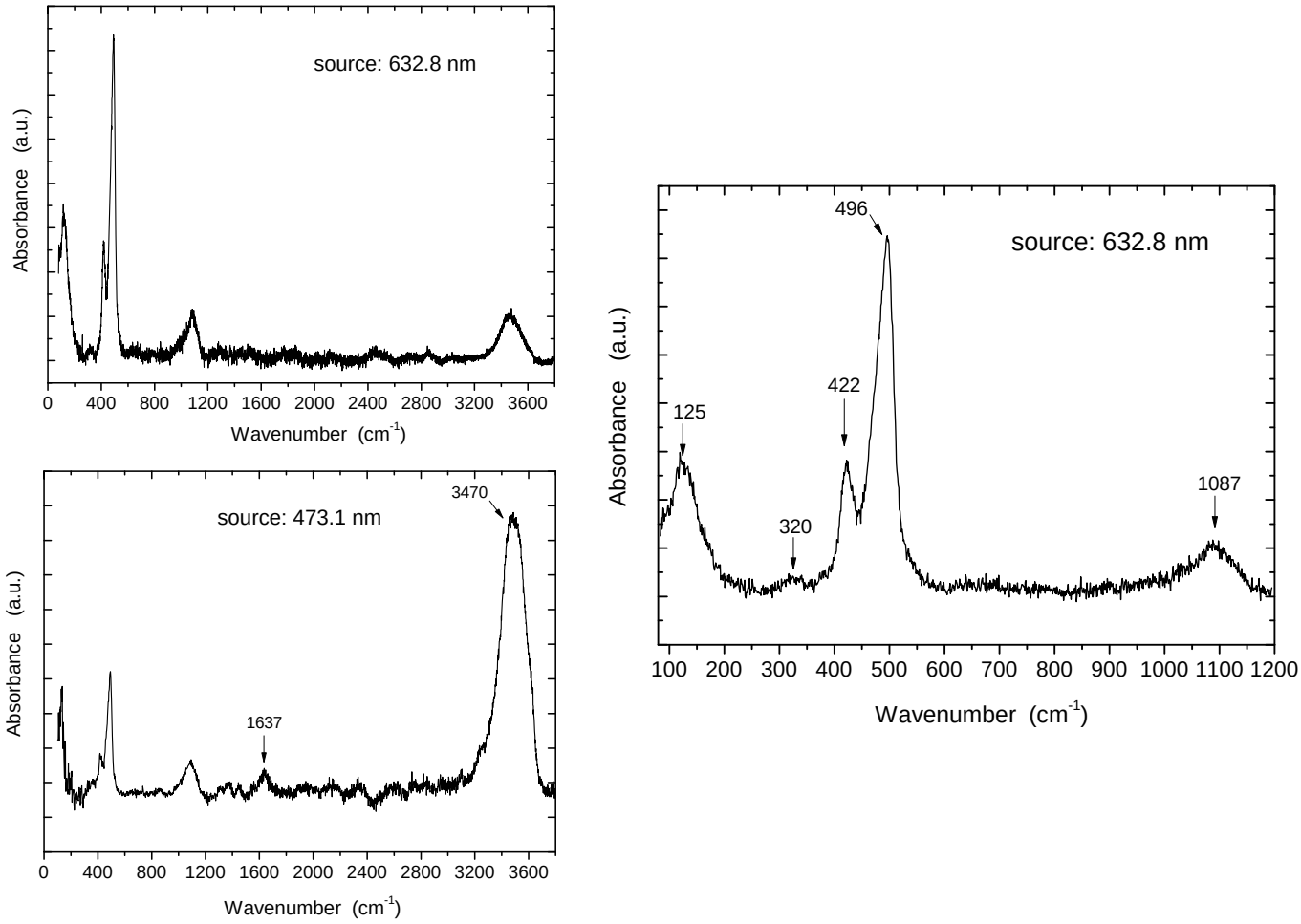

Figure 4. (*Top*) Powder mid-IR spectrum and (*down*) single-crystal near-IR spectrum of merlinoite.